



Research article

Inhibition performance of uniconazole on steel corrosion in simulated concrete pore solution: An eco-friendly way for steel protection

Yuanyuan Meng^{a,b}, Shuangxi Li^{b,*}, Zhi Zhang^c^a College of Civil Engineering & Transportation, South China University of Technology, Guangzhou, Guangdong 510640, China^b College of Hydraulic and Civil Engineering, Xinjiang Agricultural University, Urumqi, 830052, China^c Guangzhou Expressway Co, Ltd., Guangzhou, Guangdong 510000, China

ARTICLE INFO

Keywords:

Steel bar

Simulated concrete pore solution

Uniconazole

Corrosion inhibitor

Electrochemical test

ABSTRACT

Corrosion inhibitors play a vital role in impeding the corrosion process of steel bars within concrete structures exposed to corrosive environments. Nevertheless, conventional corrosion inhibitors pose environmental risks. In contrast, contemporary studies have explored corrosion inhibitors that are eco-friendly. However, these inhibitors are burdened by high costs and complex production processes, impeding the widespread application in concrete structures. Consequently, this study presents an innovative solution by incorporating uniconazole, an agricultural fungicide, as a corrosion inhibitor for steel bars in concrete structures. The steel bars were exposed to corrosion within a simulated concrete pore solution containing 0.6 mol/L NaCl, both with and without the presence of uniconazole. The morphology and hydrophilicity of the steel bar surface were investigated via optical microscope and contact angle experiments. Electrochemical tests (open circuit potential, potentiodynamic polarization, electrochemical impedance spectroscopy, and Mott-Schottky analysis) and X-ray photoelectron spectroscopy were employed to investigate the corrosion inhibition performance and mechanism of uniconazole. The results demonstrate that uniconazole elevates the hydrophobicity and contributes to the corrosion inhibition of steel bars. Electrochemical test results indicate that as the concentration of uniconazole increases from 1×10^{-4} mol/L to 1×10^{-3} mol/L, the inhibition efficiency likewise demonstrates a corresponding increase, escalating from around 50%–90%. Uniconazole molecules function as mixed-type inhibitors, exhibiting characteristics of both anode-type and cathode-type inhibitors. The adsorption of uniconazole enhances the stability and thickness of the passive-adsorbed layer on the steel surface, effectively impeding the charge transfer process and obstructing the interaction of corrosive substances with the base metal. In summary, the application of uniconazole exhibits the highlights of efficient, cost-effective, environmentally friendly, and the potential for scalable production. This positions uniconazole as a promising candidate for use as a corrosion inhibitor in the domain of concrete structures.

^{*} Corresponding author.E-mail address: xjlisx123@xjau.edu.cn (S. Li).<https://doi.org/10.1016/j.heliyon.2024.e24688>

Received 7 April 2023; Received in revised form 4 December 2023; Accepted 12 January 2024

Available online 13 January 2024

2405-8440/© 2024 The Authors. Published by Elsevier Ltd. This is an open access article under the CC BY-NC-ND license (<http://creativecommons.org/licenses/by-nc-nd/4.0/>).

1. Introduction

Steel bar is known as an indispensable material in reinforced concrete structures [1], which has a series of advantages: high economic efficiency, excellent mechanical properties, and a similar thermal expansion coefficient to concrete [2]. In concrete structures, where the pore solution is characterized by alkalinity (pH between 12.5 and 14), a stable passive film is formed on the surface of steel bars, protecting the underlying metal from the action of aggressive species. However, in concrete structures, the breakdown of passive film (also defined as depassivation) can be initiated by aggressive environments, especially in the environment rich in chloride ions (Cl^-), such as marine environments, saline environments, de-icing salt environments, etc. [3–7]. In these environments, the depassivation of steel bars can lead to expansion, corrosion, and even fracture, which raises significant safety hazards, economic losses, and environmental crises [5,8,9]. As a consequence, the corrosion of steel bars under a Cl^- -rich environment in reinforced concrete structures is regarded as a critical durability issue, posing a significant challenge [10].

Numerous studies have consistently demonstrated that the incorporation of corrosion inhibitors at low concentrations into reinforced concrete structures is widely recognized as the most effective and cost-efficient strategy for steel corrosion prevention [11–13]. Corrosion inhibitors, categorized as admixtures, demonstrate the ability to effectively prevent or delay the corrosion process of steel bars [14]. Traditional corrosion inhibitors commonly used in reinforced concrete structures include compounds like triethanolamine (TEA), benzotriazole (BTA), and their derivatives, etc. [15,16]. These corrosion inhibitors offer several advantages in terms of their molecular structure [17], such as the presence of electronegative atoms (e.g., O, N, P, and S), unsaturated bonds (e.g., double bonds and triple bonds), and conjugated functional groups or the benzene ring. These features facilitate the adsorption of corrosion inhibitors onto the steel surface through mechanisms such as electrostatic interaction or chemisorption [15], effectively retarding the corrosion process of steel.

However, it should be noted that some of these traditionally employed inhibitors have shown limited effectiveness. Mashal [18] found that the inhibition efficiency of BTA for steel bars in simulated concrete pore solution (SCPS) containing Cl^- was only 70 %. Additionally, a significant drawback associated with many conventional inhibitors is their toxicity, posing risks to both human health and the environment. The use of these inhibitors during the concrete mixing process can lead to respiratory irritations, disruptions of biochemical processes, and interference with enzyme systems within the human body [15,17,19]. Furthermore, throughout the long-term service life of concrete structures, these inhibitors may pose hazards to aquatic environments and ecosystems [20–22]. In light of these, several ecological regulations have imposed limitations on the utilization of toxic chemical inhibitors [23].

In response to the increasing demand for environmental protection and the promotion of human health, there has been a growing emphasis on the development of environment-friendly corrosion inhibitors in recent years. These innovative inhibitors include biopolymers [24], ionic liquids [25], fatty acids [26], and plant extracts [27,28]. However, these inhibitors are expensive and challenging to produce on a large scale. Moreover, concrete structural projects typically exhibit substantial volume and widespread geographical applications, making it challenging to extensively propagate these inhibitors within concrete engineering. Therefore, it is necessary and meaningful to explore a novel corrosion inhibitor, which is high-effective, environment-friendly, economical, and suitable for concrete structures.

Uniconazole, as a broad-spectrum fungicide, is extensively used in both agricultural and horticultural [29]. From a molecular structure perspective, uniconazole belongs to the same category of organic compounds as BTA, commonly referred to as azole compounds. These compounds are characterized by a five-membered ring structure containing at least two heteroatoms, one of which is nitrogen. The distinctive molecular configuration of uniconazole, featuring an electronegative nitrogen atom and a benzene ring, confers advantages in terms of the adsorption mechanism [2]. Furthermore, as an agricultural fungicide, uniconazole also possesses a set of pivotal characteristics that present significant potential for its extensive integration into large-scale concrete engineering projects. Firstly, uniconazole is readily available in the market, as it is produced by numerous pesticide manufacturers. Secondly, its competitive pricing makes it an attractive choice compared to other fungicides and pesticides [17]. Lastly, uniconazole is known for its environmentally friendly properties, which further contribute to its popularity. The distinctive attributes of uniconazole present promising prospects for utilization as a highly effective, environmentally friendly, cost-effective, and readily deployable corrosion inhibitor in concrete structures.

This study focuses on the evaluation of uniconazole as a novel corrosion inhibitor for steel bars utilized in concrete structures. Notably, this study signifies the pioneering adoption of an agricultural fungicide as a corrosion inhibitor within concrete structures. This offers a cost-effective and novel option for corrosion inhibition in concrete structures. In this study, steel bars were processed by various erosion durations and inhibitor concentrations in a Cl^- -rich SCPS environment. Furthermore, different analytical techniques were employed to comprehensively explore the corrosion inhibition performance and mechanism of uniconazole. To be specific, the morphology and hydrophilicity of the steel bars surface were investigated by optical microscopy (OM) and contact angle experiments. The anti-corrosion performance of uniconazole was thoroughly investigated by electrochemical measurements. These measurements included open circuit potential (OCP), potentiodynamic polarization (PDP), electrochemical impedance spectroscopy (EIS), and Mott-Schottky (MS) analyses. Additionally, the chemical composition of the film formed on the steel surface was investigated using X-ray photoelectron spectroscopy (XPS) measurements.

2. Experimental

2.1. Materials and reagents

Uniconazole (AR), purchased from Shanghai Yuanye Bio-Technology Co. Ltd. China, was employed as the corrosion inhibitor in the

present work. The molecular structure of uniconazole is shown in Fig. 1. The required reagents, including $\text{Ca}(\text{OH})_2$ (AR), NaCl (AR), and ethyl alcohol were obtained from Shanghai Aladdin Biochemical Technology Co., Ltd. Steel bar (Q235) was selected as the testing specimen, and its chemical composition is presented in Table 1.

2.2. Preparation of specimens

The specimen used in this study was fabricated from steel bars and was in the form of cylinders with a 4 mm length and a diameter of 10 mm [30]. To prepare these specimens, a stepwise grinding process was employed, using emery papers ranging from 240 to 1200 grades. Subsequently, the specimens were rinsed with deionized water, subjected to degreasing with ethyl alcohol, and then thoroughly dried under ambient room conditions [3]. A copper line was soldered onto one cross-section of the specimen. Moreover, to protect against corrosion, the soldered cross-section surface and side surface of the specimen was carefully sealed using epoxy resin. The other cross-section of the specimen, which was exposed to the solution during subsequent tests, retained a working area of 0.785 cm^2 .

2.3. Corrosion exposure

To simulate the concrete environment, a saturated solution of $\text{Ca}(\text{OH})_2$ was prepared using deionized water and served as the SCPS [8]. Subsequently, the specimens were immersed in the SCPS for 7 days to facilitate the formation of a stable passive film on the surface of the steel bar [31]. The OCP of the specimens was measured as a means of confirming the passive state of the steel [32]. To investigate the anti-corrosion effects of uniconazole, two distinct exposure procedures were devised. Initially, NaCl was introduced into the SCPS, resulting in a concentration of 0.6 mol/L. The specimens were exposed to this Cl^- -enriched SCPS (referred to as Cl-SCPS), which simulated the corrosion process of steel bars in an aggressive environment [3]. This corrosion exposure process was designated as the reference group and was denoted as the "Blank" group. Furthermore, corrosion inhibitor solutions (CIS) were formulated by adding various concentrations of uniconazole (1×10^{-4} mol/L, 2.5×10^{-4} mol/L, 5×10^{-4} mol/L, 7.5×10^{-4} mol/L, and 1×10^{-3} mol/L) to the Cl-SCPS. The specimens were subsequently subjected to exposure under these diverse concentrations of CIS to investigate the anti-corrosion behavior of steel bars in the presence of uniconazole. These specimens were labeled as CIS-0.1, CIS-0.25, CIS-0.5, CIS-0.75, and CIS-1.0, respectively.

2.4. Methodology

To ensure reproducibility, a minimum of three replicates were carried out for each measurement. In particular, representative curves were chosen from repetitions and are depicted in the figures. Furthermore, the test results are presented in the form of figures accompanied by error bars or as tables displaying the mean \pm standard deviation.

2.4.1. Surface morphology

After an immersion period of 30 days, the surface morphology of the specimens was examined using an optical microscope (OM) with a magnification of $175\times$. The microscope model used for the investigation was the Olympus KH7700.

2.4.2. Wettability

To assess the hydrophilic/hydrophobic properties of the specimens treated with/without uniconazole, the water contact angles experiment was conducted on the specimen's surface by an optical contact angle measuring device (Kruss DSA30, Germany) at a room temperature of 25°C . Before the tests, the specimens were exposed to solutions for 72 h.

2.4.3. Electrochemical experiment

The anti-corrosion performance of uniconazole on steel bars was assessed through a series of electrochemical tests conducted using

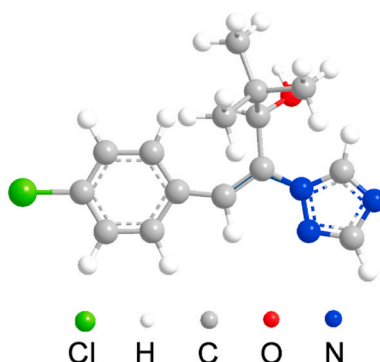


Fig. 1. Molecular structure of uniconazole.

Table 1
Chemical composition of the steel.

Element	C	S	P	Si	Mn	Fe
wt. %	0.22	0.05	0.045	0.30	0.65	balance

a PARSTAT2273 electrochemical workstation. These tests included OCP, PDP, EIS, and MS experiments. For the electrochemical measurements, a traditional three-electrode configuration electrochemical cell was employed. The platinum electrode, featuring an exposed surface area of 4 cm², was employed as the counter electrode (CE). An improved version of the saturated calomel electrode (SCE), denoted as model number 217 and manufactured by LeiCi (China, Shanghai), was employed as the reference electrode (RE). It is noteworthy that this improved version of the SCE incorporates a self-contained salt bridge design, effectively mitigating the potential direct reactions or interference between the ions present in the solution and the electrode. The test specimen functioned as the working electrode (WE). PDP, EIS, and MS tests were conducted on the specimen at different exposure durations of 6h, 12h, or 72h in solutions. Before initiating PDP, EIS, and MS measurements, the WE underwent an additional 30-min stabilization period at the OCP condition to ensure potential stability. PDP sweeps were carried out with a potential range from -250 mV to 1000 mV versus OCP, using a scan rate of 0.3 mV/s. EIS experiments were performed at the OCP, employing a sinusoidal potential perturbation of 10 mV and a frequency range varying from 10⁵ to 10⁻² Hz. The MS tests encompassed a potential range from -1.0V_{SCE} to 0.5V_{SCE}, utilizing a potential step of 20 mV/s and a frequency of 1 kHz. All electrochemical tests were performed under standard room conditions at a temperature of 25 ± 1 °C.

2.4.4. XPS analysis

The chemical composition analysis of the passive film on the surface of the steel bar was conducted by XPS tests. The tests were performed using a Thermo Scientific K-Alpha + system, which was equipped with a monochromatic Al K α X-ray source. The XPS spectra were calibrated concerning the C1s peak at a binding energy of 284.8 eV, serving as the reference for energy calibration.

3. Results

3.1. Surface morphology

The surface morphology of the specimens was examined after a 30-day immersion in a Blank solution and different concentrations

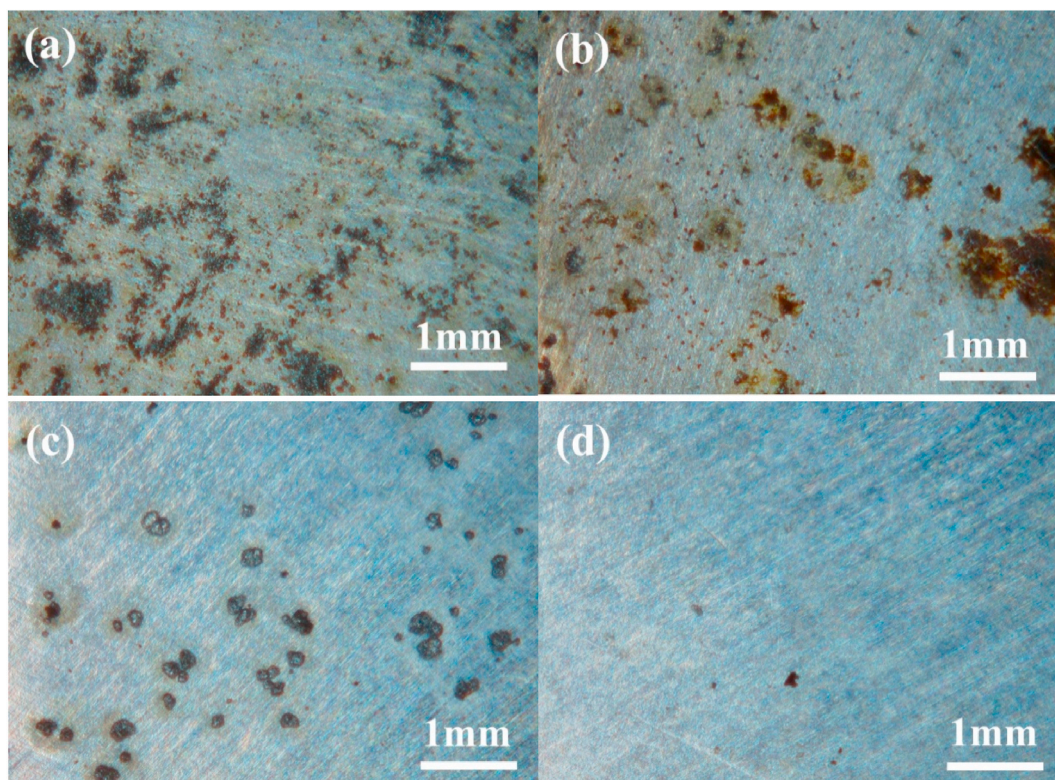


Fig. 2. Optical graph of steel bar after 30 d immersion in various solutions: (a) Blank, (b) CIS-0.1, (c) CIS-0.5, and (d) CIS-1.0.

of CIS. As shown in Fig. 2, the surface of the specimens exhibits varying degrees of corrosion pits, providing visual evidence of the corrosion-inhibiting effect of uniconazole. In the case of the specimen immersed in the solution without uniconazole (Fig. 2(a)), the surface exhibits pronounced roughness, accompanied by numerous corrosion pits. Conversely, for the specimen subject to CIS with a concentration of 1×10^{-4} mol/L uniconazole (Fig. 2(b)), there is a modest reduction in the number of corrosion pits. Furthermore, as the concentration of uniconazole in CIS increases from 5×10^{-4} mol/L (Fig. 2(c)) to 1×10^{-3} mol/L (Fig. 2(d)), the surface of the specimens progressively becomes smoother, and the quantity of corrosion pits diminishes. These observations suggest that uniconazole tends to decrease the rate of corrosion reactions and impede the progression of the corrosion process.

3.2. Water contact angle measurement

The water contact angle (θ) of the specimen's surface is an indicator of wettability. If $\theta < 90^\circ$, indicating that the specimen's surface is hydrophilic; whereas if $\theta > 90^\circ$, implying the specimen's surface is hydrophobic [33,34]. Therefore, the larger the angle, the better the specimen's hydrophobicity. Fig. 3 presents the θ results of the treated specimens by pendant drop method. It can be observed that the measured contact angle for the Blank specimen is 52.1° , significantly less than 90° . This can be attributed to the corrosive conditions, which result in surface inhomogeneity. As a result, the surface of the steel bar is easily wetted by water molecules and exhibits a hydrophilic property. Alternatively, the contact angles recorded for the specimens retrieved from the corrosion inhibitor are found to be 73.1° , 79.5° , 84.4° , 89.1° , and 93.4° for CIS-0.1, CIS-0.25, CIS-0.5, CIS-0.75, and CIS-1.0, respectively. It can be observed that the θ of the treated specimens demonstrates an increasing trend. Moreover, the higher the concentration of uniconazole, the larger the θ of specimen's surface, indicating that the hydrophobicity of the specimens' surface is enhanced by the presence of uniconazole molecules.

3.3. Open circuit potential monitoring

The initiation and progression of the corrosion process, as well as the influence of anodic or cathodic mechanisms, can be preliminarily assessed by the variation of E_{OCP} [27,28]. Fig. 4 presents the E_{OCP} -Time results for the specimens exposed to various solutions. The readings of all specimens exhibit significant downward trends and fluctuations during the initial immersion period (0 h–6 h). This observation indicates the initiation and progression of the corrosion process, nevertheless, after 6 h, the stable E_{OCP} values indicate a steady state between the proceeding of the corrosion process and the deposition of corrosion products [1].

As depicted in Fig. 4, the E_{OCP} of the specimen subjected to the Blank exposure process exhibits pronounced fluctuations. Even after a 6-h immersion, the E_{OCP} value continues to decrease, indicating an ongoing progression of corrosion. In contrast, for the specimens immersed in the solution containing uniconazole, the fluctuations of E_{OCP} are significantly reduced compared to the Blank specimen, suggesting the formation of an adsorbed film on the specimen's surface. Furthermore, as the concentration of uniconazole increases, the potential fluctuations diminish, and the time required to reach a steady state decrease. These observations indicate that more uniconazole molecules adsorb onto the steel surface, forming a denser and more stable surface film.

In particular, with the addition of uniconazole, the E_{OCP} values of the specimen shift towards more anodic. This observation suggests that the uniconazole molecule is more dominant in the anodic reaction rather than in the cathodic reaction.

3.4. Potentiodynamic polarization

PDP plots of the specimens exposed to various solutions for 6 h are displayed in Fig. 5. To demonstrate the trends of PDP curves, only a selection of the specimens' PDP curves is presented. The electrochemical parameters obtained from the PDP curves using Cview2 software are summarized in Table 2. These parameters encompass the corrosion potential (E_{corr}), corrosion current density (i_{corr}), Tafel slope of the anode (β_a) and cathode (β_c), pitting potential (E_{pit}), and corrosion efficiency (η). The i_{corr} values are calculated by extrapolating the linear region of the curves near the Tafel region to the corresponding E_{corr} . The η is calculated using the following equation:

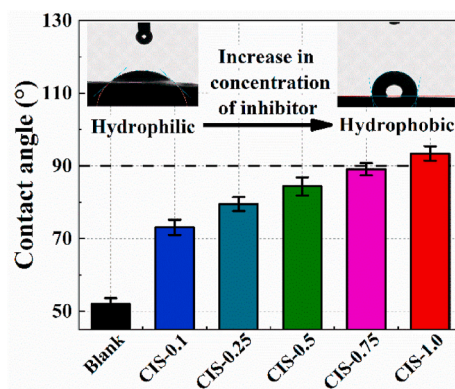


Fig. 3. Water contact angle of specimens after 72h immersion in various solutions.

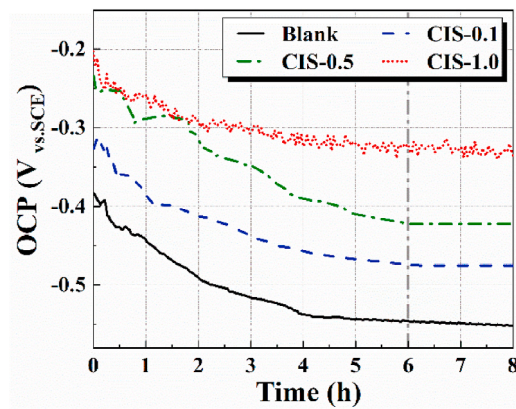


Fig. 4. OCP evolution for steel bar during the first 6 h of exposure to various solutions.

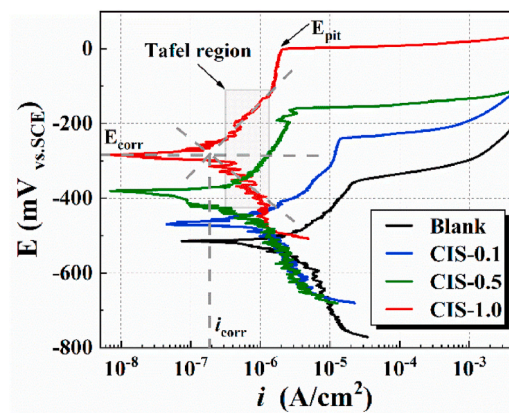


Fig. 5. PDP results of steel electrodes exposed in various solutions after 6h immersion.

Table 2

Corrosion kinetic parameters of steel electrodes processed by different exposure processes for 6 h.

Exposure process	E_{pit} (mV vs. SCE)	E_{corr} (mV vs. SCE)	i_{corr} ($\mu\text{A}/\text{cm}^2$)	β_c (mV/dec)	β_a (mV/dec)	η (%)
Blank	-360 ± 13	-518 ± 38	2.93 ± 0.7	-303 ± 24	175 ± 18	–
CIS-0.1	-241 ± 24	-472 ± 21	1.31 ± 0.3	-311 ± 16	195 ± 22	55.3
CIS-0.25	-209 ± 9	-431 ± 30	0.89 ± 0.2	-309 ± 17	205 ± 21	69.8
CIS-0.5	-163 ± 11	-380 ± 22	0.47 ± 0.1	-319 ± 11	234 ± 15	83.9
CIS-0.75	-88 ± 3	-329 ± 19	0.36 ± 0.1	-322 ± 14	249 ± 22	87.8
CIS-1.0	-1 ± 4	-286 ± 13	0.22 ± 0.1	-326 ± 10	267 ± 16	92.6

$$\eta(\%) = \frac{i_{corr} - i_{corr}}{i_{corr}} \times 100 \quad (1)$$

where i'_{corr} represents the corrosion current density of the steel electrodes in the Blank solution without uniconazole, and i_{corr} represents the corrosion current density of the steel electrodes in the CIS with uniconazole [35].

As observed from Fig. 5, all PDP curves show a passive zone in the anodic region. Within this passive zone (before reaching the point of E_{pit}), a relatively low current density is maintained. This is attributed to the spontaneous passivity exhibited by the steel bar in SCPS. In an alkaline environment like SCPS, a solid and protective oxide layer forms on the surface of the steel bar, providing resistance to anodic dissolution in the passive region. Beyond the point of E_{pit} , there is a sudden increase in the current density, owing to the breakdown of the passive film and the formation of corrosion pits. The presence of H_2O and Cl^- close to the steel surface can induce the dissolution of the passive layer. Consequently, the concentration of Cl^- on the steel surface plays a crucial role in determining the magnitude of E_{pit} . As shown in Table 2, the incorporation of uniconazole results in a significant increase in E_{pit} compared to the Blank specimen, accompanied by a marked reduction in current density. These results indicate the inhibitory impact of uniconazole on the steel bar. It is attributed to the replacement of H_2O and Cl^- from the film/metal interface by the uniconazole through the absorption-

substitution mechanism.

As illustrated in Fig. 5 and Table 2, the specimen exposed to the solution without the uniconazole exhibits the lowest E_{corr} and the highest i_{corr} . In contrast, the specimens treated with solutions containing uniconazole show a positive shift in E_{corr} and a narrower range of i_{corr} . These findings indicate the effective adsorption of uniconazole molecules onto the steel surface, thereby, uniconazole covers a greater surface area and hinders the electron flow toward the steel surface. Furthermore, as the concentration of uniconazole increases, the specimens demonstrate higher E_{corr} and lower i_{corr} . This observation suggests the formation of a denser protective film on the steel surface, which effectively mitigates the chemical attack from corrosive media. That is to say, the presence of this adsorbed film acts as a barrier, reducing the susceptibility of the steel surface to corrosion.

Furthermore, compared to the specimen immersed in the blank solution, the slopes of both β_a and β_c for the specimens undergo significant changes upon the introduction of uniconazole. This indicates that the adsorption of uniconazole on the steel surface affects both the anodic and cathodic reactions. In other words, uniconazole inhibits the oxidative dissolution of iron in the anodic region as well as the oxygen reduction in the cathodic region. Particularly, the value of β_a exhibits more pronounced fluctuations compared to β_c concerning the Blank specimen. This suggests that uniconazole can be classified as a mixed-type corrosion inhibitor with a predominant anodic action.

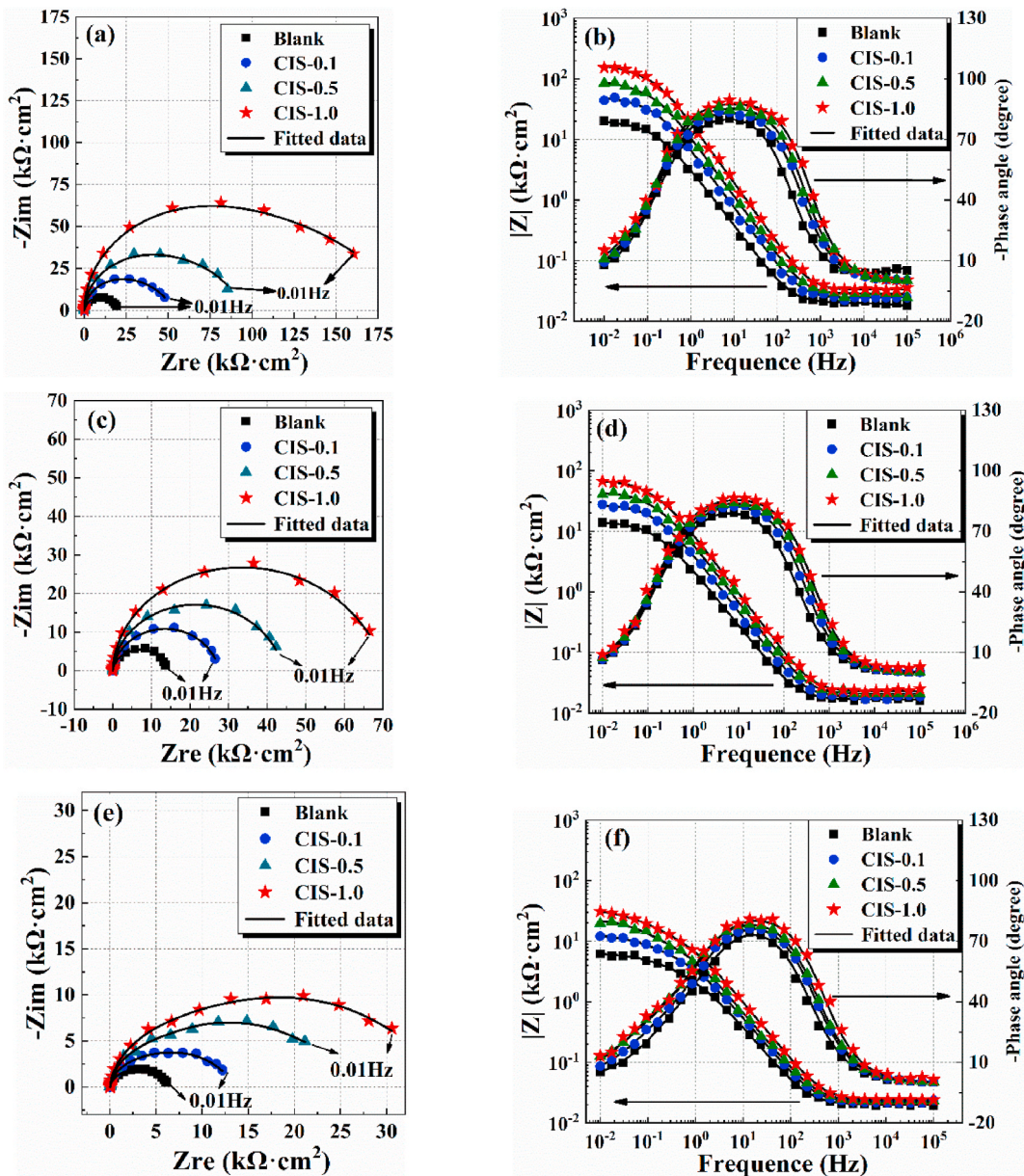


Fig. 6. Nyquist and Bode plots of steel bars exposed in Blank solution or CIS with different durations: 6h (a, b), 12h (c, d), and 72h (e, f).

As per the data presented in Table 2, when comparing the specimen processed with the Blank process, the η of the specimen immersed in the CIS shows an ascending trend. This result further indicates that uniconazole exhibits a significant corrosion inhibition capability, and this effect becomes more pronounced as the concentration increases. The maximum inhibition efficiency, exceeding 90.0 %, is achieved at a uniconazole concentration of 1×10^{-3} mol/L.

3.5. Electrochemical impedance spectroscopy

The EIS results of steel electrodes exposed to different solutions for 6h, 12h, and 72h are presented in Fig. 6, displaying Nyquist plots and Bode plots. To highlight the EIS trends, only selected curves of the specimens are presented. The obtained results showed that there is only one capacitive loop in the Nyquist plot, furthermore, the Bode plot reveals a single time constant. Such appearance in Nyquist and Bode plots is attributed to charge transfer controlled phenomenon [33]. Thus, it can be said that the uniconazole molecules undergo a charge transfer-controlled phenomenon.

In Nyquist plots, the diameter of the capacitance arc is closely associated with the corrosion inhibition performance of inhibitors. It is worth noting that an increase in the diameter of the capacitance arc indicates a more uniform and denser adsorbed film, which suggests enhanced corrosion protection. As depicted in Fig. 6(a–c, e), it can be observed that the specimens immersed in Blank solution show the lowest diameter of the capacitance arc. It is attributed to the effect of Cl^- , which destroys the passivation film on the specimen surface. Correspondingly, specimens subjected to the CIS treatment exhibit a discernible augmentation in the capacitance arc’s diameter, with this augmentation being directly proportional to the escalating concentration of uniconazole. This observation indicates that uniconazole effectively retards the corrosion process of steel bars. It can be attributed to the adsorption of uniconazole molecule, which blocks the active sites of the steel rebar surface. Additionally, the diameter of the capacitance arc gradually decreases with prolonged exposure duration, particularly for the specimens immersed in the solution without uniconazole. This decreased trend suggests the penetration of corrosive media through the passive film. Conversely, for the specimens treated with the solution containing uniconazole, the diameter of the capacitance arcs remains at a relatively high level throughout the exposure duration, indicating that the stability of the passive film may be preserved by the presence of uniconazole molecules. In accordance with previous literature [36], the slopes of the capacitance arc observed at medium frequency are associated with the resistance of the adsorbed film. In Fig. 6, it is evident that the slopes of the capacitance arc at medium frequency are significantly higher for specimens treated with inhibitors in comparison to those without inhibitors. This observation suggests the formation of a more intact adsorbed film in the presence of inhibitors. Furthermore, the Bode plots depicted in Fig. 6(b–d, f) reveal that both the modulus and phase angle gradually increase with the increment of uniconazole concentration. This upward trend also indicates a corrosion inhibitory effect of uniconazole on the steel surface.

The EIS plots (Fig. 6) were fitted using the equivalent circuit (EC) model with ZSimpWin software. The fitted results are presented in Table 3. The EC model is commonly employed to simulate the electrochemical behavior of steel in an alkaline environment [30], as depicted in Fig. 7. The EC model consists of several components. R_s represents the resistance of the electrolyte solution. Q_1 and R_1 represent the capacitance and resistance of the passive-adsorbed layer, respectively. These parameters are primarily associated with the redox reactions occurring within the passive-adsorbed layers [37]. Q_{dl} corresponds to the double-layer capacitance, which arises from the formation of an electrical double-layer when molecules are adsorbed or complexed on the steel surface. R_{ct} represents the charge transfer resistance.

In the EC model, the parameters Q_1 and Q_{dl} are substituted by a constant phase angle element (CPE), with the impedance Z_{CPE}

Table 3
Fitting parameters of the steel processed with various exposure processes.

Exposure process	R_s (Ω/cm^2)	n_r	C_1 ($\mu\text{F}/\text{cm}^2$)	R_1 ($\text{k}\Omega/\text{cm}^2$)	n_{dl}	C_{dl} ($\mu\text{F}/\text{cm}^2$)	R_{ct} ($\text{k}\Omega/\text{cm}^2$)	η (%)
6h								
Blank	19.72 ± 1	0.94 ± 0.03	34.69 ± 5	12.26 ± 2	0.76 ± 0.01	88.61 ± 10	7.59 ± 1	–
CIS-0.1	24.54 ± 3	0.96 ± 0.01	18.16 ± 3	36.13 ± 2	0.72 ± 0.01	80.37 ± 7	16.15 ± 2	53.00
CIS-0.25	22.98 ± 2	0.98 ± 0.01	16.94 ± 3	49.57 ± 6	0.75 ± 0.02	72.37 ± 8	28.56 ± 2	73.42
CIS-0.5	28.44 ± 4	0.98 ± 0.02	12.58 ± 4	63.82 ± 5	0.80 ± 0.04	67.93 ± 7	30.81 ± 2	75.37
CIS-0.75	29.05 ± 5	0.98 ± 0.01	10.26 ± 2	75.91 ± 9	0.82 ± 0.02	68.49 ± 2	69.51 ± 5	89.08
CIS-1.0	33.39 ± 6	0.99 ± 0.03	8.09 ± 1	82.00 ± 7	0.69 ± 0.02	66.25 ± 5	88.45 ± 3	91.42
12h								
Blank	16.87 ± 4	0.93 ± 0.04	36.07 ± 4	9.81 ± 1	0.70 ± 0.03	104.34 ± 4	4.21 ± 1	–
CIS-0.1	18.77 ± 2	0.96 ± 0.02	21.69 ± 5	17.26 ± 2	0.73 ± 0.01	89.10 ± 7	8.77 ± 1	52.00
CIS-0.25	20.69 ± 3	0.97 ± 0.02	20.06 ± 2	22.34 ± 2	0.76 ± 0.02	87.12 ± 6	12.59 ± 3	66.56
CIS-0.5	20.85 ± 1	0.97 ± 0.02	20.85 ± 2	29.51 ± 2	0.75 ± 0.02	80.11 ± 3	15.78 ± 2	73.32
CIS-0.75	23.56 ± 3	0.99 ± 0.04	18.59 ± 1	38.12 ± 4	0.74 ± 0.03	81.17 ± 8	22.21 ± 2	81.04
CIS-1.0	23.13 ± 4	0.98 ± 0.01	15.41 ± 3	46.76 ± 3	0.76 ± 0.01	81.03 ± 7	30.42 ± 5	86.16
72h								
Blank	20.10 ± 2	0.92 ± 0.03	52.25 ± 6	2.71 ± 1	0.66 ± 0.02	138.59 ± 11	3.74 ± 1	–
CIS-0.1	21.62 ± 1	0.93 ± 0.02	22.62 ± 4	4.99 ± 1	0.64 ± 0.02	113.50 ± 8	7.56 ± 1	50.53
CIS-0.25	23.01 ± 3	0.93 ± 0.03	21.84 ± 3	7.05 ± 2	0.72 ± 0.01	101.94 ± 9	9.63 ± 2	61.16
CIS-0.5	22.90 ± 3	0.93 ± 0.03	18.77 ± 2	9.26 ± 1	0.77 ± 0.03	89.96 ± 7	13.70 ± 5	72.70
CIS-0.75	22.58 ± 4	0.94 ± 0.01	15.66 ± 2	10.01 ± 2	0.70 ± 0.04	86.39 ± 6	20.58 ± 4	81.83
CIS-1.0	24.11 ± 2	0.95 ± 0.02	13.25 ± 2	10.94 ± 2	0.64 ± 0.04	82.95 ± 8	25.11 ± 3	85.11

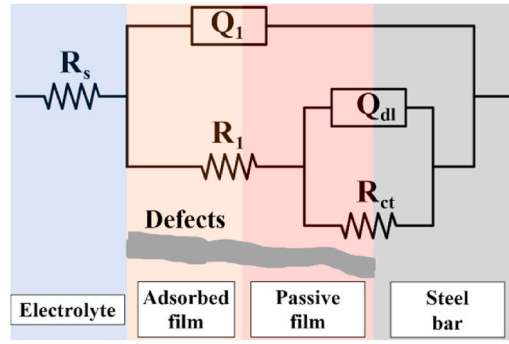


Fig. 7. Equivalent circuit (EC) model.

expressed as below:

$$Z_{CPE}(Y_0)^{-1}(j\omega)^{-n} = (Y_0)^{-1}(\omega)^{-n} \left(\cos \frac{n\pi}{2} - j \sin \frac{n\pi}{2} \right) \quad (2)$$

where Y_0 represents the basic admittance, j represents the imaginary unit, ω represents the angular frequency ($\omega = 2\pi f$), and n represents a constant [38]. Notably, the value of n ranges from 0 to 1: when $n = 0$, the CPE behaves like a resistor, when $n = 0.5$, the CPE behaves like a Warburg impedance, and when $n = 1$, the CPE behaves like a capacitor [39]. Upon reviewing the fitted parameter values presented in Tables 3 and it can be observed that $n < 1$, which signifies that the CPE does not exhibit pure capacitance behavior. Consequently, the effective capacitances (C_1 and C_{dl}) were calculated using the Brug equation, as shown in eq. (3) [30]:

$$C = Y_0^{\frac{1}{n}} \left(\frac{1}{R_{is}} + \frac{1}{R_{ip}} \right)^{\frac{n-1}{n}} \quad (3)$$

where R_{is} represents the series resistance, and R_{ip} represents the parallel resistance concerning the CPE.

The formation of the passive-adsorbed layer on the steel surface is attributed to the redox reactions involving iron ions, and the extent of this process can be evaluated by the quantity of charge transfer. The quantity of charge transfer is directly related to the value of the passive-adsorbed layer capacitance (C_1), and this relationship can be mathematically expressed as follows [40]:

$$C_1 = q \frac{d\theta}{dE} \quad (4)$$

where q represents the total amount of charge that can transform within the passive-adsorbed layer, while θ denotes the degree of transformation at a specific electrode potential. As shown in Table 3, at the same immersion duration, the value of C_1 presents a tendency to decrease with the increased concentration of uniconazole. This observation can be explained by the adsorption mechanism of uniconazole, which results in a significant reduction of the transformable charges.

As is known, the parameter R_1 is closely associated with defects (such as pores) within the passive and adsorbed film. These defects serve as direct pathways for the migration of ions and electrons. Consequently, the value of R_1 is directly correlated with the number of such defects present within the passive-adsorbed layer. Based on the data presented in Table 3, the Blank specimen exhibits the lowest value of R_1 , indicating an inadequately protective passive film on the surface of the steel bar. In contrast, the values of R_1 demonstrate an increasing trend with the increasing concentration of uniconazole. This phenomenon can be attributed to the presence of uniconazole molecules, which lead to the formation of a thicker and more resistant passive-adsorbed layer on the steel surface. Consequently, the penetration of corrosive media into the substrate steel is effectively hindered. Moreover, the value of R_1 for each specimen decreases with the prolonged immersion duration, suggesting that the passive-adsorbed layer gradually becomes more susceptible to penetration by corrosive media.

In accordance with the Helmholtz model, the thickness and capacitance of the double layer are interrelated and can be described by the following equation [41]:

$$C_{dl} = \frac{\epsilon^0 \epsilon}{d} S \quad (5)$$

where ϵ^0 represents the vacuum dielectric constant, ϵ refers to the dielectric constant of the electrolyte within the capacitor, S represents the exposed surface area of the working electrode, and d represents the thickness of the double layer. Based on the data presented in Table 3, with the addition of uniconazole, the C_{dl} of the specimens shows a decreasing trend. This observation can be attributed to the replacement of corrosive media at the metal-solution interface by uniconazole molecules, leading to an increase in the thickness of the double layer. Additionally, as the immersion time increases, the C_{dl} tends to increase. This phenomenon is ascribed to the gradual penetration of corrosive media into the steel surface, resulting in an increase in the exposed surface area and a decrease in the thickness of the double-layer.

Derived from the findings delineated in Table 3, a salient observation emerges as the Blank specimen manifests the lowest R_{ct} value, signifying an inadequately protective oxide layer on the surface of the steel bar. Conversely, the R_{ct} value of the electrodes immersed in CIS displays an increasing trend, indicating the corrosion-inhibiting properties of uniconazole. This phenomenon can be attributed to the adsorption of uniconazole, which develops a protective film on steel surfaces. Thus, an additional resistance owing to the adsorption of uniconazole is referred to as film resistance. Furthermore, with the prolongation of the immersion duration, the R_{ct} values of all specimens exhibit a decreasing trend, suggesting that the specimens are gradually corroded under the attack of corrosive media.

To further demonstrate the inhibitory effect of uniconazole, the inhibition efficiency ($\eta\%$) of different concentrations of uniconazole at various immersion durations is calculated using the following equation:

$$\eta\% = \frac{R_{ct} - R_{ct}^0}{R_{ct}} \times 100 \tag{6}$$

where R_{ct} and R_{ct}^0 represent the charge transfer resistance with and without uniconazole, respectively. As presented in Table 3, the highest $\eta\%$ reaches 91.42 %. The results further reveal that uniconazole shows a significant corrosion-inhibiting property on the surface of the steel bar. The values obtained from EIS measurement are found to be in the same trend as obtained from the PDP study. It is evident that the results obtained from both these techniques are corroborating well.

3.6. Semiconducting property

The passive film on the surface of the steel, consisting of iron oxides, exhibits semiconducting characteristics. To investigate the semiconducting behavior of the passive film, capacitance measurements were conducted. The specimens, which were immersed in CIS with different concentrations of uniconazole for a duration of 72h, were subjected to measurements. The results of MS plots are depicted in Fig. 8. The negative slope observed in MS plots (at the potential beneath $-0.8 \text{ V}_{vs. SCE}$) indicates a p-type semiconducting oxide layer [42]. Meanwhile, the positive slope observed in MS plots (within the potential ranges from $-0.6 \text{ V}_{vs. SCE}$ to $0.5 \text{ V}_{vs. SCE}$) refers to an n-type semiconducting oxide layer [43].

The measured capacitance (C) and electrode potential (E) conform to the MS equation, which accommodates the series combination of the space charge depletion layer (C_{sc}) and the Helmholtz layer (C_{dl}) [44], as elucidated by eq. (7). It is important to note that the space charge depletion layer comprises anionic vacancies and iron bases, whereas the adsorption of uniconazole molecules onto the passive film induces the formation of the Helmholtz layer through physical or chemical interactions.

$$\frac{1}{C} = \frac{1}{C_{sc}} + \frac{1}{C_{dl}} = \begin{cases} \sqrt{\frac{2\left(E - E_{FB} + \frac{kT}{q}\right)}{ee_0qN_A}} + \frac{1}{C_{dl}} & \text{p-type semiconductor} \\ \sqrt{\frac{2\left(E - E_{FB} - \frac{kT}{q}\right)}{ee_0qN_D}} + \frac{1}{C_{dl}} & \text{n-type semiconductor} \end{cases} \tag{7}$$

In general, C_{dl} is much higher than that of C_{sc} and can be neglected. Thus, the MS equation can be simplified as follows [45]:

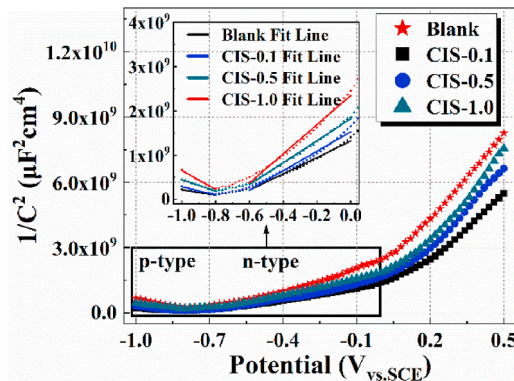


Fig. 8. MS plots of the oxide layer on the steel surface after a 72h immersion in different exposure processes.

$$\frac{1}{C^2} = \begin{cases} \frac{2 \left(E - E_{FB} + \frac{kT}{q} \right)}{ee_0qN_A} & \text{p-type semiconductor} \\ \frac{2 \left(E - E_{FB} - \frac{kT}{q} \right)}{ee_0qN_D} & \text{n-type semiconductor} \end{cases} \quad (8)$$

where E_{FB} represents the flat band potential, which is determined by the intersection of the fitting line with the X-axis. The parameter k denotes the Boltzmann constant ($k = 1.38 \times 10^{-23}$ J/K), T represents the absolute temperature, q represents the elementary charge ($q = 1.602 \times 10^{-19}$ C), e represents the dielectric constant of the passive film ($e = 15.6$), and e_0 represents the vacuum permittivity ($e_0 = 8.854 \times 10^{-14}$ F/cm). Furthermore, N_A and N_D correspond to the acceptor density and donor density, respectively. The values of N_A and N_D were determined through the fitting analysis of the negative (-1.0 to -0.8 V_{vs. SCE}) and positive (-0.6 to 0.0 V_{vs. SCE}) slopes, as illustrated in the enlarged section of Fig. 8.

The computed parameters derived from the MS analysis are presented in Table 4. Examination of the table reveals a trend wherein the concentrations of uniconazole exhibit an inverse relationship with both N_D and N_A . Notably, N_D plays a significant role in determining the stability of the passive film, as a higher N_D value indicates a more susceptible passive film to corrosion. Consequently, the decrease in N_D values with the increasing concentration of uniconazole in CIS implies the effective corrosion inhibition induced by the presence of uniconazole molecules, safeguarding the steel bar against corrosive processes.

According to Freire [40], Fe(II) is identified as the primary donor for the passive film formed on steel bars in an alkaline environment. Hence, the decrease in N_D can be attributed to a reduction in the Fe(II) content within the passive film. The decrease in Fe(II) content is likely a consequence of the interaction between the uniconazole molecules and Fe(II) when they adsorb onto the passive film.

3.7. Chemical composition of the passive-adsorbed layer

The chemical composition of the passive-adsorbed layer plays a significant role in determining the corrosion resistance of steel bars. To gain insights into the inhibitory mechanism of uniconazole on steel bars immersed in CIS, the valence state of iron ions and nitrogen atoms within the steel's passive-adsorbed layer was investigated using XPS. The specimens were immersed in CIS with varying concentrations of uniconazole for a duration of 72 h. The XPS survey spectra of the specimens are presented in Fig. 9. As depicted in the figure, the spectra of the specimen treated with the Blank solution exhibit recognizable peaks corresponding to the C1s, O1s, and Fe2p regions. Moreover, the presence of the N element can be observed on the specimens treated with CIS, indicating the adsorption of uniconazole molecules on the steel's surface. This observation can be ascribed to the adsorption mechanism.

The Fe 2p_{3/2} spectra of the steel surface were acquired following a 72-h exposure to different solutions, as shown in Fig. 10. These Fe 2p_{3/2} spectra were deconvoluted into three distinct contributions: Fe⁰ (706.8 eV) [46], Fe(II) oxide (709.6 eV) [47], and Fe(III) oxide (711.5 eV) [48]. Fig. 10 portrays the variations in the iron ion species within the passive-adsorbed layer of the steel bar, as influenced by different concentrations of uniconazole.

It is well-known that XPS has a detection depth limit of 10 nm. Therefore, the presence of Fe⁰ in the results suggests that the thickness of the passive-adsorbed layer is below this 10 nm threshold. The decrease in Fe⁰ content indicates an increase in the thickness of the passive-adsorbed layer, comprising both a passive film and an adsorbed film, thereby establishing a double protective layer. Based on the observations delineated in Fig. 11, the gradual reduction in Fe⁰ content due to the introduction of uniconazole implies the adsorption of uniconazole on the steel surface, leading to the formation of a thicker protective layer.

In comparison to the specimens treated with the Blank solution, the incorporation of uniconazole induces alterations in the chemical composition of the passive-adsorbed layer on the steel surface, as depicted in Fig. 11. Firstly, the specimens treated with CIS exhibit a notable reduction in the Fe(II) content, which aligns with the observed decrease in donor density in the MS plots. Furthermore, there is a noteworthy increase in the Fe(III) content, transitioning from 34.51 % to 65.87 %. This variation can be attributed to the chemisorption of uniconazole on the steel surface, leading to the formation of Fe-uniconazole compounds. Consequently, the proportion of iron oxide content within the passive film undergoes a discernible transformation.

In accordance with prior research findings [15,49], an increase in the Fe(II) content within the passive-adsorbed layer results in the generation of a higher number of oxygen vacancies within this layer, thus upholding charge equilibrium. This, in turn, enhances the stability of the passive film, as indicated by an increasing Fe(III)/Fe(II) ratio. In the current investigation, the Fe(III)/Fe(II) ratios for

Table 4

MS parameters of the passive film on steel after 72h immersion in various exposure processes.

Exposure process	p-type semiconductive			n-type semiconductive		
	E_{fb} (V)	N_A (10^{21} cm ⁻³)	R^2	E_{fb} (V)	N_D (10^{21} cm ⁻³)	R^2
Blank	-0.62 ± 0.02	15.84 ± 1.5	0.97	-0.71 ± 0.01	4.89 ± 0.5	0.99
CIS-0.1	-0.69 ± 0.03	10.04 ± 2.0	0.97	-0.70 ± 0.02	4.12 ± 0.8	0.98
CIS-0.5	-0.65 ± 0.02	7.13 ± 0.8	0.99	-0.74 ± 0.02	3.64 ± 0.1	0.99
CIS-1.0	-0.69 ± 0.02	4.25 ± 0.2	0.99	-0.71 ± 0.01	2.75 ± 0.1	0.99

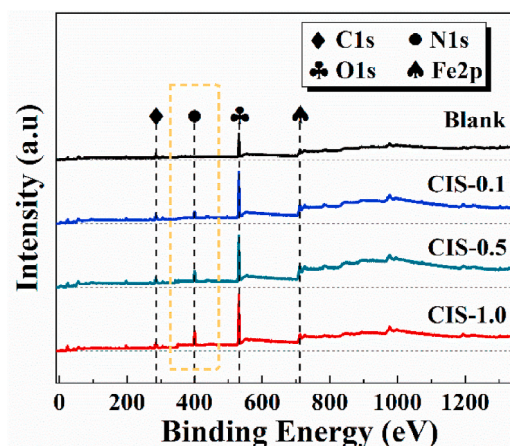


Fig. 9. XPS survey spectra of the steel bar treated by different processes after 72 h of immersion.

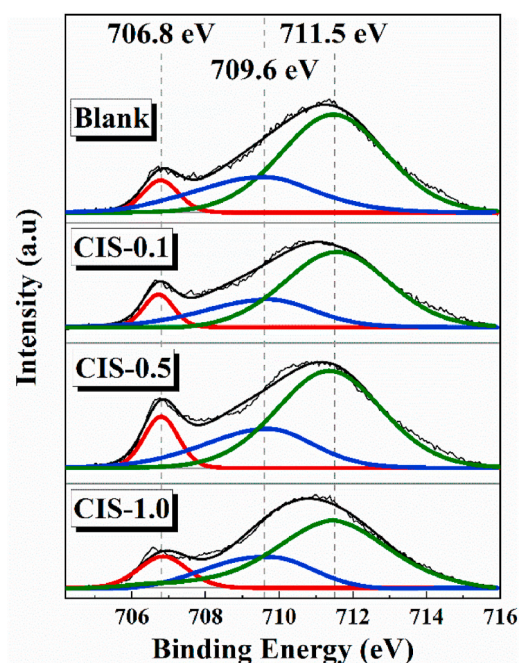


Fig. 10. High-resolution Fe $2p_{3/2}$ spectra for steel after 72 h immersion in different exposure processes.

the specimens treated in solutions with varying uniconazole concentrations of 0 , 0.1×10^{-4} , 0.5×10^{-4} , and 1.0×10^{-4} mol/L are calculated to be 0.65, 2.19, 2.58, and 2.71, correspondingly, demonstrating an increasing trend. Consequently, the stability and thickness of the passive film are enhanced with the increase in uniconazole concentration.

The narrow scan spectra of N 1s on the surface of the steel bar are subjected to analysis. The N 1s spectrum can be fitted to the peaks at 399.9 eV and 407.1 eV (Fig. 12). These peaks are attributable to the =N- [8,50] and the bond between N heteroatoms and C atoms [51] of uniconazole molecule. Notably, the response of these peaks exhibited a direct correlation with the concentration of uniconazole. It is noteworthy that the intensity of these peaks displayed an ascending trend with the increasing concentration of uniconazole. This observation provides further evidence of the adsorption of uniconazole on the steel surface and the concentration-dependent increase in the thickness of the adsorbed layer. This observation furnishes additional substantiation for the phenomenon of uniconazole adsorption on the steel surface and the concurrent concentration-dependent augmentation in the thickness of the adsorbed layer.

4. Comparative analysis of similar inhibitors

Currently, there is a wide variety of corrosion inhibitors. In order to provide a clearer elucidation of uniconazole's advantages,

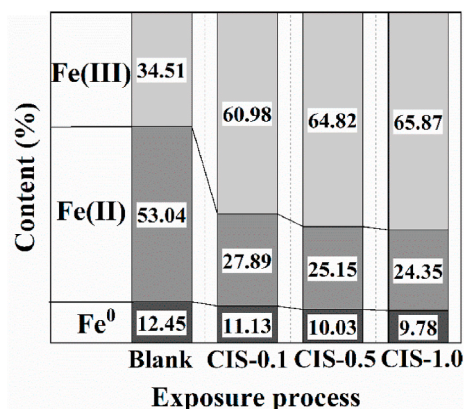


Fig. 11. Variations about iron ion on the passive-adsorbed layer of steel processed by various exposure processes after 72 h immersion.

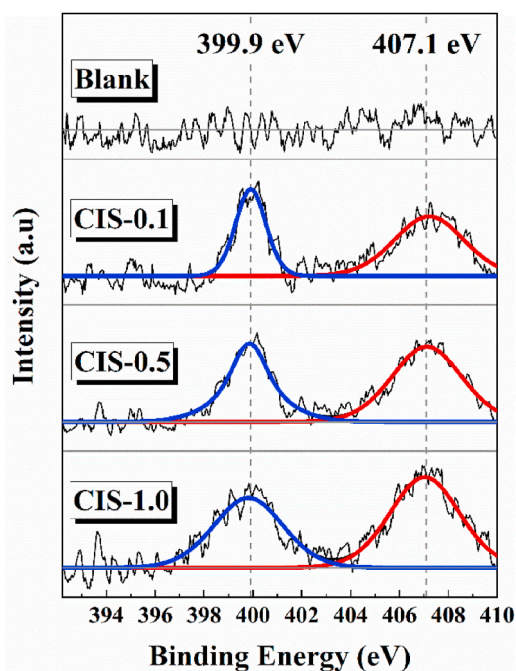


Fig. 12. High-resolution N 1s spectra for steel immersed in various solutions after 72h.

Table 5
Comparative of the similar inhibitors.

Property	Traditional corrosion inhibitors	Innovative corrosion inhibitors	
	TEA, BTA, and their derivatives, etc.	Biopolymers, ionic liquids, fatty acids, plant extracts, etc.	Uniconazole
Inhibition efficiency	Medium [18,52]	High [24,53]	High
Environmental friendliness	Harmful [17]	Friendly [27]	Friendly [29]
Health hazards to humans	Harmful [15]	Friendly [28]	Friendly [29]
Production complexity	/	Complex [25,26]	Easy [17]
Cost	/	High [25,26]	Low [17]

Table 5 compares the properties of various corrosion inhibitors (including traditional ones, newly highlighted inhibitors in recent years, and uniconazole) across different aspects.

According to Table 5, uniconazole demonstrates unique advantages such as ease of production, cost-effectiveness, environmental friendliness, and high inhibition efficiency. These attributes encompass all the characteristics required for large-scale concrete

engineering. This suggests that uniconazole, an agricultural fungicide, holds promising potential for widespread adoption as a corrosion inhibitor in concrete structures.

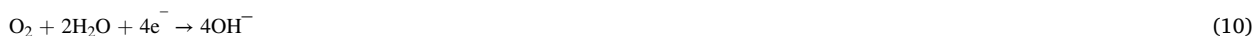
5. Discussion

Within concrete structures, which often exhibit an alkaline environment, steel bars spontaneously undergo the formation of a thin and compacted passive film. This passive film, primarily consisting of iron oxides, functions as a protective barrier, effectively preventing direct interaction between the steel bars and aggressive media such as O_2 , H_2O , and others present in the surrounding environment. However, when the steel bars are exposed to these aggressive environments, an electrochemical cell is initiated, comprising an anode region and a cathode region:

Anode reaction:



Cathode reaction:



In a chloride-rich environment, Cl^{-} can permeate the concrete matrix, thereby instigating a chemical reaction with the passive film present on the steel bar surface [54]:



Based on the reactions delineated above, it is noteworthy that the free Cl^{-} function exclusively as catalysts at the surface of steel bar, undergoing repeated interactions with the steel substrate. The introduction of Cl^{-} disrupts the stability of the passive film, consequently leading to the exposure of the underlying steel substrate.

These electrochemical reactions initiate a corrosion process in the steel bars. It is important to note that corrosion exhibits a self-propagating process, wherein its progression tends to accelerate over time. Iron oxides present on the steel surface exhibit a strong affinity for Cl^{-} . The affinity serves to augment the corrosion process, culminating in heightened exposure of the steel bar and an escalated rate of corrosion. This progressive corrosion ultimately results in the deterioration of the reinforced concrete structure.

Based on the findings of this study, it is evident that the incorporation of uniconazole within the Cl-SCP exhibits a proficient inhibition of steel bar corrosion. This favorable outcome can be attributed to the adsorption mechanism, which can be discerned from the experimental results derived from PDP, EIS, and XPS analyses. The distinctive molecular structure of uniconazole, characterized by its abundance of N atoms and aromatic segments, facilitates the adsorption process and the consequent establishment of an adsorption film on the steel bar surface. The adsorption mechanism of uniconazole onto the steel surface in a corrosive environment is depicted in Fig. 13. It is well-established that the dielectric constant of the organic molecules is lower in comparison to that of both H_2O and Cl^{-} . As a result, uniconazole molecules are capable of adsorbing onto the steel surface, displacing the previously adsorbed H_2O and Cl^{-} . The adsorbed uniconazole molecule act as an inhibitive barrier, effectively retarding or preventing the corrosion reactions taking place at the steel solution interface. Consequently, the thickness of the electrical double layer increases and the corrosion process slows down. Moreover, as the concentration of uniconazole molecules increases, a greater number of uniconazole molecules become available for adsorption on the steel bar surface. This expanded coverage of the surface area results in enhanced inhibition efficiency. The adsorption mechanism of the uniconazole molecules may occur in the following forms.

(1) Physisorption

From a molecular charge density perspective, uniconazole exhibits a predominant concentration of valence electron cloud around its heteroatoms (N, O, and Cl) and conjugated double bonds. This molecular characteristic contributes to a robust electrostatic adsorption phenomenon on the surface of the steel bar. Additionally, the presence of large π -bonds within the benzene ring of uniconazole facilitates the polar adsorption of the molecules onto the steel surface [10]. Consequently, an adsorbed film composed of uniconazole molecules forms on the steel surface, leading to an improvement in the quality of the passive film.

(2) Chemisorption

On the other hand, the variations in the content of different valence states of iron ions on the passive-adsorbed layer, as confirmed through XPS analysis (Fig. 11), provide compelling evidence for the occurrence of chemisorption. This phenomenon arises due to the N atom within the azole structure of uniconazole, which possesses numerous lone pair electrons capable of donating electrons to the empty d orbital of Fe atoms. Thus, resulting in the formation of donor-acceptor complexes. Furthermore, the aromatic segments of uniconazole can both donate and accept electrons from the Fe atoms, further enhancing the chemisorption process. In essence, the chemisorption induced by uniconazole molecules leads to the formation of insoluble Fe-uniconazole compounds on the surface of the passive film. Consequently, the presence of uniconazole molecules facilitates the development of a thicker and more integrated

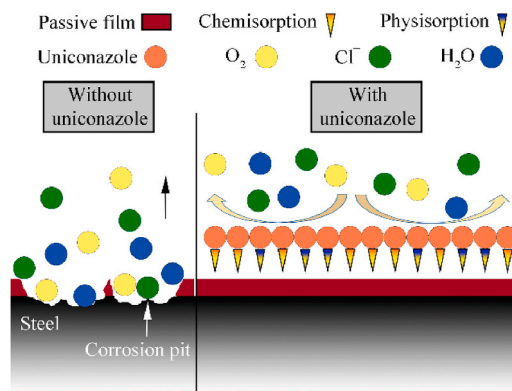


Fig. 13. Schematic diagrams of the inhibition mechanism of uniconazole for steel bar.

adsorbed film on the steel surface.

In summary, uniconazole molecules may exhibit both physisorption and chemisorption bonding with the steel surface. The uniconazole molecules, along with the formed Fe-uniconazole compounds, create a protective barrier on the steel surface. This barrier effectively impedes the ingress of corrosive media such as O_2 , Cl^- , and H_2O , thereby impeding the cathode reaction (described in Eq. (10)). Furthermore, the presence of uniconazole molecules leads to a state of equilibrium with the Fe ions, resulting in a stabilized condition. In this state, the affinity of Fe ions towards Cl^- is reduced [37]. As a result, the penetration of Cl^- becomes more challenging, thus slowing down the reaction rate of iron dissolution triggered by Cl^- [7]. In other words, the anodic reaction depicted in Eq. (9) is mitigated.

The preceding discussion on the adsorption forms of uniconazole (physisorption and chemisorption) is based on inferences drawn from electrochemical test results and XPS analysis. Further confirmation of its corrosion inhibition mechanisms is imperative from the perspective of uniconazole's electronic and molecular properties [33,55]. For instance, investigating the modes of interaction between uniconazole (electronic and molecular) and steel surfaces, as well as the adsorption mechanism that uniconazole exerts on the steel surfaces at both the electronic and molecular levels. To address these issues, the next stage of research will involve a more comprehensive analysis using molecular dynamics methods to explore the corrosion inhibition mechanism of uniconazole from electronic and molecular viewpoints.

6. Conclusions

The uniconazole, as a kind of highly efficient and environment-friendly corrosion inhibitor on steel surfaces in Cl-SCPS, was investigated by OM, electrochemical measurements, adsorption isotherm, and XPS. The conclusions drawn from the study can be summarized as follows.

- (1) Uniconazole demonstrates corrosion inhibition properties on the steel surface in Cl-SCPS. The effectiveness of inhibition increases with the concentrations of uniconazole, while it decreases with prolonged immersion duration. The maximum inhibition efficiency, exceeding 90 %, is achieved at a concentration of 1×10^{-3} mol/L.
- (2) Uniconazole acts as a mixed-type inhibitor, effectively inhibiting both the oxidative dissolution in the anodic region and the oxygen reduction in the cathodic region of the steel bar.
- (3) The adsorption of uniconazole molecules on the steel surface results in the formation of an adsorption film, which effectively impedes the penetration of corrosive media and provides protection to the base metal.
- (4) The interaction between uniconazole and steel surface results in the formation of Fe-uniconazole compounds. This phenomenon reduces the donor density and facilitates the subsequent oxidation process from Fe(II) to Fe(III). Consequently, a thicker and more stable passive-adsorbed layer is formed on the steel surface.

Data availability statement

Data will be made available on request.

CRediT authorship contribution statement

Yuanyuan Meng: Writing – review & editing, Writing – original draft, Methodology, Investigation, Formal analysis, Data curation, Conceptualization. **Shuangxi Li:** Supervision, Resources, Funding acquisition, Conceptualization. **Zhi Zhang:** Validation, Resources, Project administration, Data curation.

Declaration of competing interest

The authors declare that they have no known competing financial interests or personal relationships that could have appeared to influence the work reported in this paper.

Acknowledgments

This work was supported by the National Natural Science Foundation of China (52508704).

References

- [1] H.M. Abd El-Lateef, M.M. Khalaf, M. Gouda, et al., Novel water-soluble organoselenocyanates and symmetrical diselenides tethered N-succinylamide and N-maleanilamide as corrosion inhibitors for reinforced steel in the simulated concrete pore solution, *Constr. Build. Mater.* 366 (2023) 130135, <https://doi.org/10.1016/j.conbuildmat.2022.130135>.
- [2] Q. Wang, X. Wu, H. Zheng, et al., Evaluation for Fatsia japonica leaves extract (FJLE) as green corrosion inhibitor for carbon steel in simulated concrete pore solutions, *J. Build. Eng.* 63 (2023) 105568, <https://doi.org/10.1016/j.jobee.2022.105568>.
- [3] C. Xiong, W. Li, Z. Jin, et al., Preparation of phytic acid conversion coating and corrosion protection performances for steel in chlorinated simulated concrete pore solution, *Corros. Sci.* 139 (2018) 275–288, <https://doi.org/10.1016/j.corsci.2018.05.018>.
- [4] S.W. Tang, Y. Yao, C. Andrade, et al., Recent durability studies on concrete structure, *Cement Concrete Res* 78 (2015) 143–154, <https://doi.org/10.1016/j.cemconres.2015.05.021>.
- [5] Y. Li, Y.F. Cheng, Passive film growth on carbon steel and its nanoscale features at various passivating potentials, *Appl. Surf. Sci.* 396 (2017) 144–153, <https://doi.org/10.1016/j.apsusc.2016.11.046>.
- [6] S. Mundra, M. Criado, S.A. Bernal, et al., Chloride-induced corrosion of steel rebars in simulated pore solutions of alkali-activated concretes, *Cement Concrete Res* 100 (2017) 385–397, <https://doi.org/10.1016/j.cemconres.2017.08.006>.
- [7] K. Subbiah, H.S. Lee, S. Mandal, et al., Conifer cone (pinus resinosa) as a green corrosion inhibitor for steel rebar in chloride-contaminated synthetic concrete pore solutions, *ACS Appl. Mater. Interfaces* 13 (36) (2021) 43676–43695, <https://doi.org/10.1021/acsami.1c11994>.
- [8] T. Xiang, Y. Zhang, L. Cui, et al., Synergistic inhibition of benzotriazole and sodium D-gluconate on steel corrosion in simulated concrete pore solution, *Colloid. Surface.* 661 (2023) 130918, <https://doi.org/10.1016/j.colsurfa.2023.130918>.
- [9] G. Ma, J. Xu, L. Han, et al., Enhanced inhibition performance of NO₂-intercalated MgAl-LDH modified with nano-SiO₂ on steel corrosion in simulated concrete pore solution, *Corros. Sci.* 204 (2022) 110387, <https://doi.org/10.1016/j.corsci.2022.110387>.
- [10] Y. Zhao, Y. Chen, X. Li, et al., The use of TEA-H₃PO₄ and TEA-C₁₈H₃₀O₃S as eco-friendly corrosion inhibitors in cementitious materials: an experimental and theoretical study, *Cement Concrete Res* 165 (2023) 107073, <https://doi.org/10.1016/j.cemconres.2022.107073>.
- [11] A. Nazari, B. Ramezanzadeh, L. Guo, et al., Application of green active bio-molecules from the aquatic extract of Mint leaves for steel corrosion control in hydrochloric acid (1M) solution: surface, electrochemical, and theoretical explorations, *Colloid. Surface.* 656 (2023) 130540, <https://doi.org/10.1016/j.colsurfa.2022.130540>.
- [12] L. Cui, M. Hang, H. Huang, et al., Experimental study on multi-component corrosion inhibitor for steel bar in chloride environment, *Constr. Build. Mater.* 313 (2021) 125533, <https://doi.org/10.1016/j.conbuildmat.2021.125533>.
- [13] X. Zhou, M. Li, X. Guan, et al., Insights into the enhanced corrosion resistance of carbon steel in a novel low-carbon concrete with red mud and phytic acid, *Corros. Sci.* 211 (2023) 110903, <https://doi.org/10.1016/j.corsci.2022.110903>.
- [14] A. Goyal, E. Ganjian, H.S. Pouya, et al., Inhibitor efficiency of migratory corrosion inhibitors to reduce corrosion in reinforced concrete exposed to high chloride environment, *Constr. Build. Mater.* 303 (2021) 124461, <https://doi.org/10.1016/j.conbuildmat.2021.124461>.
- [15] Y. Zhao, T. Pan, X. Yu, et al., Corrosion inhibition efficiency of triethanolammonium dodecylbenzene sulfonate on Q235 carbon steel in simulated concrete pore solution, *Corros. Sci.* 158 (2019) 1–12, <https://doi.org/10.1016/j.corsci.2019.108097>.
- [16] K. Sabet Bokati, C. Dehghanian, Adsorption behavior of 1H-benzotriazole corrosion inhibitor on aluminum alloy 1050, mild steel and copper in artificial seawater, *J. Environ. Chem. Eng.* 6 (2) (2018) 1613–1624, <https://doi.org/10.1016/j.jece.2018.02.015>.
- [17] H. Tian, W. Li, B. Hou, Novel application of a hormone biosynthetic inhibitor for the corrosion resistance enhancement of copper in synthetic seawater, *Corros. Sci.* 53 (10) (2011) 3435–3445, <https://doi.org/10.1016/j.corsci.2011.06.025>.
- [18] M. Sheban, M. Abu-Dalo, A. Ababneh, et al., Effect of benzotriazole derivatives on the corrosion of steel in simulated concrete pore solutions, *Anti-Corros. Method. M.* 54 (3) (2007) 135–147, <https://doi.org/10.1108/00035590710748605>.
- [19] P.B. Raja, M.G. Sethuraman, Natural products as corrosion inhibitor for metals in corrosive media — a review, *Mater. Lett.* 62 (1) (2008) 113–116, <https://doi.org/10.1016/j.matlet.2007.04.079>.
- [20] Y. Liu, Z. Wang, X. Chen, et al., Synthesis and evaluation of omeprazole-based derivatives as eco-friendly corrosion inhibitors for Q235 steel in hydrochloric acid, *J. Environ. Chem. Eng.* 10 (6) (2022) 108674, <https://doi.org/10.1016/j.jece.2022.108674>.
- [21] L.T. Popoola, Progress on pharmaceutical drugs, plant extracts and ionic liquids as corrosion inhibitors, *Heliyon* 5 (2) (2019) e01143, <https://doi.org/10.1016/j.heliyon.2019.e01143>.
- [22] F. Kaya, R. Solmaz, İ.H. Geçibesler, Investigation of adsorption, corrosion inhibition, synergistic inhibition effect and stability studies of Rheum ribes leaf extract on mild steel in 1 M HCl solution, *J. Taiwan Inst. Chem. Eng.* 143 (2023) 104712, <https://doi.org/10.1016/j.jtice.2023.104712>.
- [23] S. Hooshmand Zaferani, M. Sharifi, D. Zaarei, et al., Application of eco-friendly products as corrosion inhibitors for metals in acid pickling processes – a review, *J. Environ. Chem. Eng.* 1 (4) (2013) 652–657, <https://doi.org/10.1016/j.jece.2013.09.019>.
- [24] I. Nadi, Z. Belattmania, B. Sabour, et al., Sargassum muticum extract based on alginate biopolymer as a new efficient biological corrosion inhibitor for carbon steel in hydrochloric acid pickling environment: gravimetric, electrochemical and surface studies, *Int. J. Biol. Macromol.* 141 (2019) 137–149, <https://doi.org/10.1016/j.ijbiomac.2019.08.253>.
- [25] E. Kamali Ardakani, E. Kowsari, A. Ehsani, Imidazolium-derived polymeric ionic liquid as a green inhibitor for corrosion inhibition of mild steel in 1.0 M HCl: experimental and computational study, *Colloid. Surface.* 586 (2020) 124195, <https://doi.org/10.1016/j.colsurfa.2019.124195>.
- [26] L. Wu, J. Wu, Z. Zhang, et al., Corrosion resistance of fatty acid and fluoroalkylsilane-modified hydrophobic Mg-Al LDH films on anodized magnesium alloy, *Appl. Surf. Sci.* 487 (2019) 569–580, <https://doi.org/10.1016/j.apsusc.2019.05.121>.
- [27] F. Kaya, R. Solmaz, İ. Halil Geçibesler, The use of methanol extract of Rheum Ribes (İşğın) flower as a natural and promising corrosion inhibitor for mild steel protection in 1 M HCl solution, *J. Ind. Eng. Chem.* 122 (2023) 102–117, <https://doi.org/10.1016/j.jiec.2023.02.013>.
- [28] F. Kaya, R. Solmaz, İ.H. Geçibesler, Adsorption and corrosion inhibition capability of Rheum ribes root extract (İşğın) for mild steel protection in acidic medium: a comprehensive electrochemical, surface characterization, synergistic inhibition effect, and stability study, *J. Mol. Liq.* 372 (2023) 121219, <https://doi.org/10.1016/j.molliq.2023.121219>.
- [29] Y. Hattori, K. Nagai, S. Furukawa, et al., The ethylene response factors SNORKEL1 and SNORKEL2 allow rice to adapt to deep water, *Nature* 460 (7258) (2009) 1026–1031, <https://doi.org/10.1038/nature08258>.
- [30] J. Xu, Q. Tan, Y. Mei, Corrosion protection of steel by Mg-Al layered double hydroxides in simulated concrete pore solution: effect of SO₄²⁻, *Corros. Sci.* 163 (2020) 108223, <https://doi.org/10.1016/j.corsci.2019.108223>.

- [31] A. Poursae, C.M. Hansson, Reinforcing steel passivation in mortar and pore solution, *Cement Concrete Res* 37 (7) (2007) 1127–1133, <https://doi.org/10.1016/j.cemconres.2007.04.005>.
- [32] C. Alonso, M. Castellote, C. Andrade, Chloride threshold dependence of pitting potential of reinforcements, *Electrochim. Acta* 47 (2002) 3469–3481, [https://doi.org/10.1016/S0013-4686\(02\)00283-9](https://doi.org/10.1016/S0013-4686(02)00283-9).
- [33] S. Sengupta, M. Murmu, S. Mandal, et al., Competitive corrosion inhibition performance of alkyl/acyl substituted 2-(2-hydroxybenzylideneamino)phenol protecting mild steel used in adverse acidic medium: a dual approach analysis using FMOs/molecular dynamics simulation corroborated experimental findings, *Colloid. Surface.* 617 (2021) 126314, <https://doi.org/10.1016/j.colsurfa.2021.126314>.
- [34] S.K. Saha, P. Banerjee, Introduction of newly synthesized Schiff base molecules as efficient corrosion inhibitors for mild steel in 1 M HCl medium: an experimental, density functional theory and molecular dynamics simulation study, *Mater. Chem. Front.* 2 (9) (2018) 1674–1691, <https://doi.org/10.1039/c8qm00162f>.
- [35] W. Li, Q. He, C. Pei, et al., Experimental and theoretical investigation of the adsorption behaviour of new triazole derivatives as inhibitors for mild steel corrosion in acid media, *Electrochim. Acta* 52 (22) (2007) 6386–6394, <https://doi.org/10.1016/j.electacta.2007.04.077>.
- [36] D. Wang, J. Ming, J. Shi, Enhanced corrosion resistance of rebar in carbonated concrete pore solutions by Na₂HPO₄ and benzotriazole, *Corros. Sci.* 174 (2020) 108830, <https://doi.org/10.1016/j.corsci.2020.108830>.
- [37] F. Teymouri, I. Samiei, S.R. Allahkaram, et al., Passive film alteration of reinforcing steel through [MoO₄²⁻]/[RCOO⁻] interfacial co-interaction for enhanced corrosion resistance in chloride contaminated concrete pore solution, *J. Mol. Liq.* 356 (2022) 119060, <https://doi.org/10.1016/j.molliq.2022.119060>.
- [38] A. Dehghani, F. Poshtiban, G. Bahlakeh, et al., Fabrication of metal-organic based complex film based on three-valent samarium ions-[bis (phosphonomethyl) amino] methylphosphonic acid (ATMP) for effective corrosion inhibition of mild steel in simulated seawater, *Constr. Build. Mater.* 239 (2020) 117812, <https://doi.org/10.1016/j.conbuildmat.2019.117812>.
- [39] J. Xu, L. Jiang, F. Xing, Influence of N,N'-dimethylaminoethanol as an inhibitor on the chloride threshold level for corrosion of steel reinforcement, *Mater. Corros.* 61 (9) (2010) 802–809, <https://doi.org/10.1002/maco.200905393>.
- [40] L. Freire, M.J. Carmezim, M.G.S. Ferreira, et al., The passive behaviour of AISI 316 in alkaline media and the effect of pH: a combined electrochemical and analytical study, *Electrochim. Acta* 55 (21) (2010) 6174–6181, <https://doi.org/10.1016/j.electacta.2009.10.026>.
- [41] D.K. Yadav, M.A. Quraishi, Application of some condensed uracils as corrosion inhibitors for mild steel: gravimetric, electrochemical, surface, morphological, UV-visible, and theoretical investigations, *Ind. Eng. Chem. Res.* 51 (46) (2012) 14966–14979, <https://doi.org/10.1021/ie301840y>.
- [42] S. Fujimoto, H. Tsuchiya, Semiconductor properties and protective role of passive films of iron base alloys, *Corros. Sci.* 49 (1) (2007) 195–202, <https://doi.org/10.1016/j.corsci.2006.05.020>.
- [43] X. Feng, X. Lu, Y. Zuo, et al., The effect of deformation on metastable pitting of 304 stainless steel in chloride contaminated concrete pore solution, *Corros. Sci.* 103 (2016) 223–229, <https://doi.org/10.1016/j.corsci.2015.11.022>.
- [44] N.E. Hakiki, S. Boudin, B. Rondot, et al., The electronic structure of passive films formed on stainless steels, *Corros. Sci.* 37 (11) (1995) 1809–1822, [https://doi.org/10.1016/0010-938x\(95\)00084-w](https://doi.org/10.1016/0010-938x(95)00084-w).
- [45] L. Ding, A. Poursae, The impact of sandblasting as a surface modification method on the corrosion behavior of steels in simulated concrete pore solution, *Constr. Build. Mater.* 157 (2017) 591–599, <https://doi.org/10.1016/j.conbuildmat.2017.09.140>.
- [46] X. Weng, Z. Chen, Z. Chen, et al., Clay supported bimetallic Fe/Ni nanoparticles used for reductive degradation of amoxicillin in aqueous solution: characterization and kinetics, *Colloid. Surface.* 443 (2014) 404–409, <https://doi.org/10.1016/j.colsurfa.2013.11.047>.
- [47] J.X. Fan, Y.J. Wang, T.T. Fan, et al., Effect of aqueous Fe(II) on Sb(V) sorption on soil and goethite, *Chemosphere* 147 (2016) 44–51, <https://doi.org/10.1016/j.chemosphere.2015.12.078>.
- [48] Y. Zhuang, Z. Zhang, T. Li, et al., XPS and XRD study of FeCl₃-graphite intercalation compounds prepared by arc discharge in aqueous solution, *Spectrochim. Acta Mol. Biomol. Spectrosc.* 70 (5) (2008) 1060–1064, <https://doi.org/10.1016/j.saa.2007.10.031>.
- [49] X. Feng, R. Shi, X. Lu, et al., The corrosion inhibition efficiency of aluminum tripolyphosphate on carbon steel in carbonated concrete pore solution, *Corros. Sci.* 124 (2017) 150–159, <https://doi.org/10.1016/j.corsci.2017.05.018>.
- [50] Y. Qiang, L. Guo, H. Li, et al., Fabrication of environmentally friendly Losartan potassium film for corrosion inhibition of mild steel in HCl medium, *Chem. Eng. J.* 406 (2021) 126863, <https://doi.org/10.1016/j.cej.2020.126863>.
- [51] X. Jiao, X. Xia, P. Liu, et al., Nickel cobaltite nanosheets strongly anchored on boron and nitrogen co-doped graphene for high-performance asymmetric supercapacitors, *Nanotechnology* 28 (31) (2017) 315403, <https://doi.org/10.1088/1361-6528/aa7ab9>.
- [52] M. Hang, M. Jiang, J. Xu, et al., The electrochemical performance and modification mechanism of the corrosion inhibitor on concrete, *Sci. Eng. Compos. Mater.* 28 (1) (2021) 352–562, <https://doi.org/10.1515/secm-2021-0037>.
- [53] Y. Liu, Z. Song, W. Wang, et al., Effect of ginger extract as green inhibitor on chloride-induced corrosion of carbon steel in simulated concrete pore solutions, *J. Clean. Prod.* 214 (2019) 298–307, <https://doi.org/10.1016/j.jclepro.2018.12.299>.
- [54] S.P. Karthick, S. Muralidharan, V. Saraswathy, et al., Long-term relative performance of embedded sensor and surface mounted electrode for corrosion monitoring of steel in concrete structures, *Sensor. Actuator. B Chem.* 192 (2014) 303–309, <https://doi.org/10.1016/j.snb.2013.10.123>.
- [55] A. Kokalj, Molecular modeling of organic corrosion inhibitors: calculations, pitfalls, and conceptualization of molecule–surface bonding, *Corros. Sci.* 193 (2021) 109650, <https://doi.org/10.1016/j.corsci.2021.109650>.